Applied Geomatics (2025) 17:393–400
https://doi.org/10.1007/s12518-025-00622-w

RESEARCH

Ground-based InSAR and GNSS integration for enhanced dam monitoring

Matthieu Rebmeister[2] · Andreas Schenk[1] · Jakob Weisgerber[3] · Malte Westerhaus[3] · Stefan Hinz[1] · Frédéric Andrian[4] · Maxime Vonié[4]

Received: 25 February 2025 / Accepted: 13 March 2025 / Published online: 26 March 2025

Abstract

The monitoring of dams is essential to ensure their safe operation for the production of renewable energy. Common tools to monitor dams are permanently installed plumblines and surveying by means of total station and leveling within a geodetic network. The main drawback of these methods is their limited spatial and temporal resolution. Recent studies have shown promising results using Ground-Based InSAR for geodetic dam monitoring. The fast acquisition speed combined with the surface monitoring capabilities enable to monitor several hundreds to thousands of points on the dam every day or several times a day. However, GB-SAR is a relative phase-measurement technique, and any interruption in the data acquisition leads to difficulties to unwrap differential phase observations and join the disjunct time series. The combination with other absolute measurement tools is promising to create an absolute deformation map of the dam. GNSS is a very efficient and reliable method providing point-wise absolute displacement time series and mm-accuracy. This paper proposes a combination of GNSS and GB-SAR observations to enhance the consistency of the surface-based dam displacement maps obtained by solely GB-SAR measurements. A method to detect unwrapping errors over long time series is proposed. The corrected GB-SAR time displacement maps are compared to a numerical model and confirm the correctness of the applied corrections.

Keywords GB-SAR · InSAR · GNSS · Dam · Monitoring

✉ Matthieu Rebmeister
matthieu.rebmeister@leica-geosystems.com

✉ Andreas Schenk
andreas.schenk@kit.edu

Jakob Weisgerber
jakob.weisgerber@kit.edu

Malte Westerhaus
malte.westerhaus@kit.edu

Stefan Hinz
stefan.hinz@kit.edu

Frédéric Andrian
frederic.andrian@arteliagroup.com

Maxime Vonié
maxime.vonie@arteliagroup.com

1 Institute of Photogrammetry and Remote Sensing, KIT, Karlsruhe 76128, Germany

2 Leica Geosystems, Heerbrugg 9435, Switzerland

3 Geodetic Institute Karlsruhe, KIT, Karlsruhe 76128, Germany

4 Artelia, Echirolles 38130, France

Introduction

In the context of climate change, dams play a critical role in generating renewable energy, as hydropower is a low-carbon and baseload alternative to fossil fuels. The continuous power output from dams can help stabilize grids, increasingly reliant on intermittent sources like solar and wind. Being a large infrastructure, often located in challenging topographic locations, the safe operation of dams requires a comprehensive monitoring concept, satisfying several criteria. Among them, temporal resolution, spatial resolution, accuracy, robustness as well as weather and daylight independency are the most important. In Scaioni et al. (2018), the possible methodologies and instruments for dam monitoring are presented. Among them, the classical and operative methods encompass plumblines, strainmeters as well as geodetic networks. While they have been validated for decades, they also present some lacks. For example, plumblines are very expensive and a limited number per dam is available, meaning that the spatial resolution is low.

In Jacquemart and Meier (2014); Wieser et al. (2020) and Rebmeister et al. (2023), the opportunities and challenges of using a Ground-based SAR system for continuous dam monitoring have been pointed out. Offering a very high temporal and spatial resolution combined with a high accuracy and a large field of view, it appears as an ideal monitoring device. Several researches exhibited the potential of GB-SAR for dam monitoring, e.g. Tarchi et al. (1999); Alba et al. (2008); Qiu et al. (2020) and Wang et al. (2020). However, the phase unwrapping, the atmospheric correction as well as the geocoding are technical challenges that have retained a long-term operational use of this type of instrument. In Rebmeister (2024), major points of these challenges have been addressed with some limitations still present. A recurring challenge is the spatial and temporal referencing or integration of double differential GB-SAR observations. The spatial referencing refers to the fixing of observational differences to points or areas, known to be stable and thus without any displacement or fixing to other geodetic observational points with known temporal displacement. The temporal referencing is challenging when the continuous temporal phase unwrapping cannot be ensured. This is the case when acquisitions are missed out for a longer period (more than several days), i.e. when hardware errors or maintenance breaks occur.

A combination with other measurement geodetic measurements can be beneficial in order to increase the reliability and robustness of the output of the GB-SAR. In this sense, robotic total stations or GNSS antennas can be considered. In Hassan et al. (2018), the comparison of GNSS and GB-SAR data has been proposed on dataset of 27 hours for rockfall monitoring. On this time span, the consistency between the two sensors has been validated and pointed out the strong influence of the atmospheric correction used for the GB-SAR data. In Bertone et al. (2023), GB-SAR and GNSS data have also shown a good consistency for glacier monitoring, over several days of observation. However, in both papers, there is no method developed to combine these data over a time span of several months. In this letter, we provide a method to use the absolute displacement time series of the GNSS to correct potential unwrapping errors in the GB-SAR processing.

Methodology

Study case

The study area is the Enguri Dam in Georgia. With a height of 271.5 m, it stands at the fifth highest arch dam in the world (ICOLD 2020). A GB-SAR has been installed as well as four GNSS antennas on the dam's crest. The GB-SAR is located at a distance of 800 m from the dam and it covers 2/3 of the complete dam structure. The GB-SAR has been running between April 2023 and June 2024, with a major interruption between December 2023 and April 2024. Due to a hardware instability, only three GNSS antennas sent data on a sufficient overlap with the GB-SAR data. From the three remaining antennas, one has been placed on the upstream side of the dam, meaning that the integration with the GB-SAR is not meaningful.

Individual data processing

GB-SAR processing

The methodology of the GB-SAR processing is shortly detailed in the following subsection. Details on each step can be found in Rebmeister (2024).

- Scene and Pixel Selection: With the system used, a new acquisition is available every 2 minutes. However scenes can be corrupted or highly influenced by atmospheric disturbances that will lead to unwrapping errors. For dam monitoring, one acquisition per day is sufficient. Therefore the first task is to find the adequate scenes and points to build the interferometric network. Criterion like amplitude dispersion (Ferretti et al. 2001) and coherence (Bamler and Hartl 1998) are used. The scenes with the highest SNR for each day are between 1 a.m. and 5 a.m. at night. They are considered for an averaged daily observation. The output of this step is one acquisition per day.
- Geocoding: The geocoding is the projection of the 2D SAR points onto an external 3D model to get the 3D coordinates of the observed pixel. A Bayesian method combined with a ray-tracing algorithm presented in Rebmeister et al. (2022) is used.
- Phase Unwrapping: An SBAS (Berardino et al. 2002) approach is used to build a redundant interferometric network. SNAPHU (Chen and Zebker 2001) is exploited to unwrap all of the interferograms. Finally, the integration of the SBAS network is achieved with the L_1-minimization. The integration of the phase via this minimization criterion reduces considerably the propagation of unwrapping errors inside the SBAS graph.
- Coherence Check: To ensure the consistency of the integrated phase, the temporal coherence between the raw master-slave interferograms and the integrated time series is computed and only points with a coherence higher than 0.98 are kept.
- Atmospheric Correction: Due to the configuration of the observed points, an extrapolation of a range-height model would lead to inaccurate results. Therefore, a simple range model (Noferini et al. 2005) is used (Rebmeister 2024).

The results of this processing are time series of 77 days between September 1st and November 4th 2023, 11 days between February 22nd and March 15th 2024, and 98 days between April 24th and July 31st, 2024 on 2226 points on the dam.

GNSS processing

Four permanent single frequency GNSS stations were strategically positioned along the dam's crest, each mounted on pre-existing, robust pillars to ensure long-term stability and reliability. As already mentioned, only three antennas have sufficient overlap with the GB-SAR time series. Since April 2023, these stations have recorded GNSS phase observations at 30-second intervals, tracking signals from both GPS and GLONASS satellites. The stations operate on a single frequency. The use of these receivers was driven by project-specific constraints, as they were already available within the project and were not required elsewhere.

The data is processed using the Wa2 module of the WaSoft software package (Wanninger and Wallstab-Freitag 2007), which applies phase-based differential processing with a reference station located approximately 1.5 km away. This differential approach is key to minimizing common GNSS errors, such as those caused by atmospheric disturbances, satellite clock inaccuracies, and orbital errors. Despite the use of single frequency receivers, the short baseline is expected to contribute to the reduction of residual tropospheric and ionospheric effects. Furthermore, multipath effects are expected to be low due to the surrounding environmental conditions. One of the GNSS stations on the dam, as well as the reference station, is equipped with a Chokering antenna, further improving signal quality by mitigating multipath interference.

The processed data results in three-dimensional coordinates for each of the three stations on the dam's crest, with daily solutions. The achieved accuracy of the 3D coordinates is in the low millimeter range, making this method highly effective for precise monitoring of the dam's deformations and structural integrity over time.

Figure 1 shows a 3D model obtained via UAV photogrammetry. The position of the GB-SAR as well as the PS displacement between September 1st and October 20th, 2023 is represented. The reference point is marked with a magenta triangle. The three GNSS antennas on the dam's crest are marked with green triangles and the displacement vectors corresponding to the above mentioned dates are represented with blue arrows.

The two antennas located on the right side of the dam are very close to each other. Moreover, one of them is located on the upstream part of the dam's crest, meaning that it has a different behavior than the observed PS points. Therefore, only two GNSS antennas will be used and referred to as the left and right antennas.

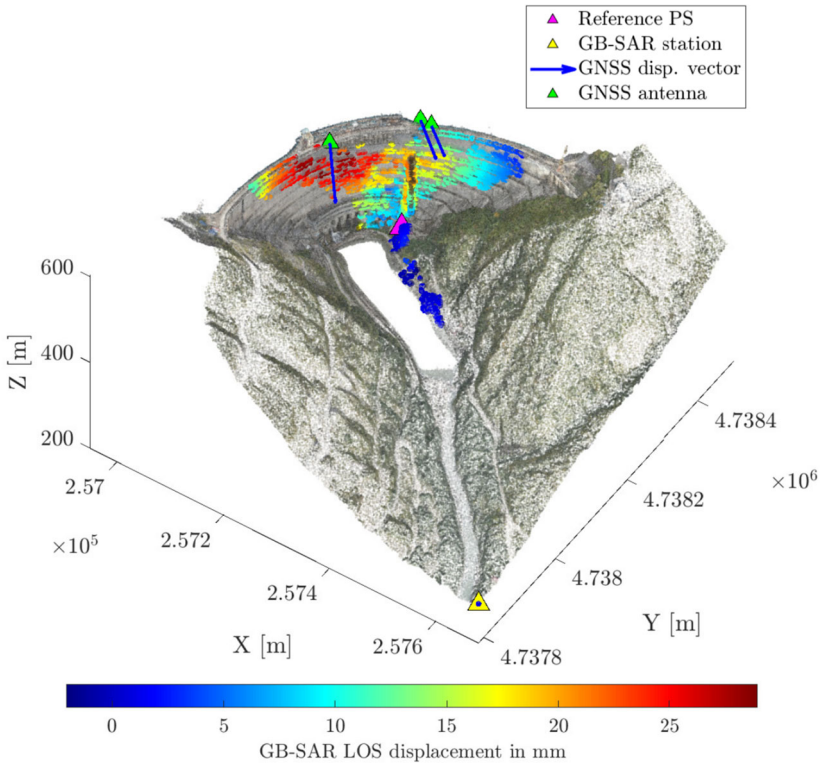

Fig. 1 Setup and data acquired at Enguri Dam with displacements shown between September 1st and October 20th, 2023

Figure 2 presents the data available at the left GNSS antenna and its nearest PS point. While the time series are close from each other at the beginning of the GB-SAR time series, they are diverging when a gap in the GB-SAR data appears between December 2023 and March 2024. As this offset is constant, it indicates one or multiple potential unwrapping errors.

Numerical model

The numerical model of the dam is used in this paper to validate the proposed approach. It is based on a mesh of the dam, with several material properties estimated, like the Young modulus. These properties are estimated by calibrating displacement with given external forces and comparing the difference between the model and the actual displacements. The data used for this calibration are the displacements of the eight plumblines inside the dam, from 2000 to 2019. More information about the computation of the model can be recovered in Rebmeister et al. (2023). The numerical model available gives the displacements observed on the whole dam structure for several epochs.

Combination method

Introduction

Satellite InSAR and GNSS combination is a research topic that started with the solution presented by Gudmundsson et al. (2002). There are usually several GNSS antennas that are distributed inside the area covered by the satellite images. Therefore, the classical processing strategies involve Bayesian interpolation method like Kriging. This process has two main goals which are the referencing on the InSAR displacement and the interpolation of the 3D displacement field.

However, in the case presented here, the spatial distribution of the GNSS antennas does not allow to conduct a meaningful interpolation and corresponds more to an extrapolation. Therefore, GNSS antennas will only be used to adjust the displacement map obtained by GB-SAR measurements. The methodology is focused on referencing GB-SAR measurements to absolute values and detecting unwrapping errors that could occur, especially when the data acquisition of the GB-SAR is interrupted.

The first task consists in searching the nearest PS point for each GNSS antenna. After that, the GNSS 3D displacements time series are projected onto the LOS of the GB-SAR and interpolated to the GB-SAR time series epochs. The alignment also deletes samples when a period of more than one day occurs without a measurement of at least one instrument.

Mathematical model for unwrapping error correction

The combination consists in solving a time series problem. Considering that we have N samples where GNSS and GB-SAR data are available. Then, the time samples are denoted with the vector $\mathbf{t}$ and the GNSS and GB-SAR displacements are respectively denoted with $\mathbf{d}_{\text{GNSS}}$ and $\mathbf{d}_{\text{GBSAR}}$. The difference is computed as $\Delta\mathbf{d} = \mathbf{d}_{\text{GNSS}} - \mathbf{d}_{\text{GBSAR}}$.

The goal of the task is to find the corrected vector $\mathbf{d}^{\text{corr}}_{\text{GBSAR}} = d^{\text{corr}}_{\text{GBSAR}}(j) \;\; \forall\, j \in \{1, ..., N\}$, given by:

$$d^{\text{corr}}_{\text{GBSAR}}(j) = d_{\text{GBSAR}}(j) + \frac{\lambda}{2}\sum_{i=1}^{j} k_i \tag{1}$$

where $\mathbf{k} = (k_1, \ldots, k_N)$ is the vector of integer phase jumps to correct unwrapping errors. The factor $\lambda/2$ is related to the conversion of 2π into millimeters using the GB-SAR wavelength λ.

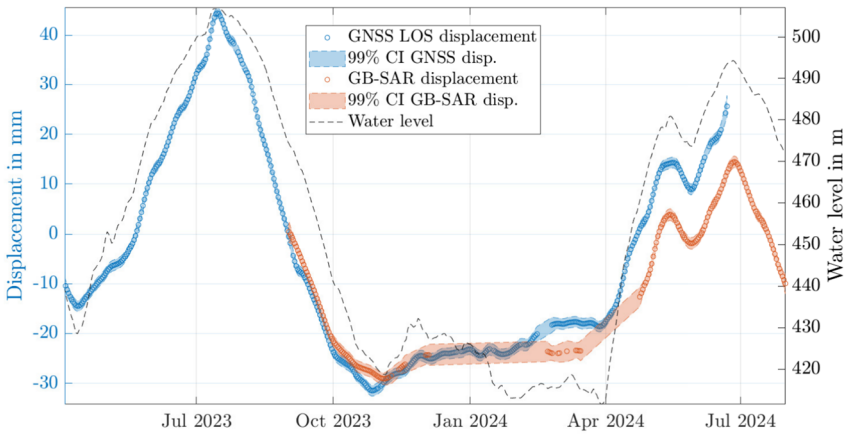

Fig. 2 Time series of the left GNSS antenna projected onto the GB-SAR LOS and nearest PS point displacement. A positive displacement indicates movement towards downstream

The cost function to minimize is therefore given by:

$$\mathcal{C}_p(\mathbf{k}) = \sum_{j=1}^{N} \left(\Delta d(j) + \frac{\lambda}{2} \sum_{i=1}^{j} k_i \right)^2, \tag{2}$$

where $\Delta d(j)$ represents the difference between the GNSS and GB-SAR displacements for the j-th sample:

$$\Delta d(j) = d_{\text{GNSS}}(j) - d_{\text{GBSAR}}(j). \tag{3}$$

The goal is to determine the vector of corrections $\mathbf{k} = (k_1, \ldots, k_N)$ that minimizes $\mathcal{C}_p(\mathbf{k})$, subject to the constraint that $k_i \in \mathbb{Z}$ (i.e., each k_i must be an integer). This ensures that the corrected GB-SAR displacements, $\mathbf{d}^{\text{corr}}_{\text{GBSAR}}$, align as closely as possible with the GNSS displacements.

In the case where several GNSS antennas are available through the observed scenario, it might happen that the estimated vectors of corrections for each GNSS antenna are not consistent. This case could occur possible when unwrapping errors happen through the interferograms. In this scenario, such spatial unwrapping errors are not expected to occur, as the geometry and the deformation pattern are smooth. Therefore, the cost function is modified to estimate only one vector of correction for all GNSS antennas.

Considering M as the number of GNSS antennas, the overall cost function is defined as:

$$\mathcal{C}(\mathbf{k}) = \sum_{p=1}^{M} \mathcal{C}_p(\mathbf{k}) \tag{4}$$

The minimization problem leads to the estimated vector of correction as:

$$\mathbf{k}^\star = \arg\min_{\mathbf{k} \in \mathbb{Z}^N} \mathcal{C}(\mathbf{k}). \tag{5}$$

After determining the optimal correction vector $\mathbf{k}^\star$, the corrected GB-SAR displacements can be calculated by applying it to all interferograms.

$$\mathbf{d}^{\text{corr}}_{\text{GBSAR}} = \mathbf{d}_{\text{GBSAR}} + \frac{\lambda}{2}\mathbf{k}^\star \tag{6}$$

This estimation aims to correct plausible phase jumps caused by interruptions in data acquisition. Since GB-SAR data maintain internal consistency through coherence evaluation at the end of processing pipeline, corrections are only applied when gaps in the GB-SAR data exceed a predefined threshold. This condition is incorporated as a constraint in the optimization process.

After this correction, there is still a residual offset value between the GNSS antenna displacements $\mathbf{d}_{\text{GNSS}}$ and the corrected GB-SAR displacements $\mathbf{d}^{\text{corr}}_{\text{GBSAR}}$. Depending on the configuration, different interpolation methods can be used. In the presented scenario and due to the presence of only two GNSS antennas available, an inverse distance weighting interpolation is applied.

Results

This section aims at presenting the results, first of the unwrapping corrections and then comparing it to the numerical model.

Time series correction

Figure 3 represents the results of the time series correction. When looking at graphics (a), it is clear that the left GNSS station and GB-SAR data have a good agreement until December 2023. The small offset between the time series can be explained by two major factors. Firstly, the measured points with the GNSS and the closest GB-SAR points are not coincident, but differ about 6 meters, and secondly, the GB-SAR time series is relative to the reference point, which may undergo some minimal movements. After the time interruption between December 2023 and March 2024, a divergence appears but lower than the half of a phase jump. Then, the offset present in May 2024 is corrected by one phase jump, which then merges well the GNSS and GB-SAR time series.

The right GNSS station (c) expresses a different behavior. Starting from the beginning until December 2023, the two time series diverge slowly. As the coherence of the GB-SAR time series as well as the temporal sampling are very high, it can be excluded that the offset originates from an unwrapping error. However, this part of the dam suffers from layover, meaning that the information in the GB-SAR is the sum of displacement signals from different parts of the dam. Still, the gap is considerably reduced by solving the unwrapping error in April 2024 as well.

Comparison with a numerical model

Three displacement maps are compared to the available numerical model:

- Uncorrected: corresponds to the original displacement map
- Corrected uw. errors: corresponds to the GB-SAR displacements with the unwrapping errors corrected.
- Corrected + interpolated: corresponds to the GB-SAR displacements with the unwrapping errors corrected as well as the interpolation of the residues.

The model is composed of about 5118 points on the dam, which reduces to 2403 points for the overlapping area imaged with the GB-SAR. The three GB-SAR displacement maps

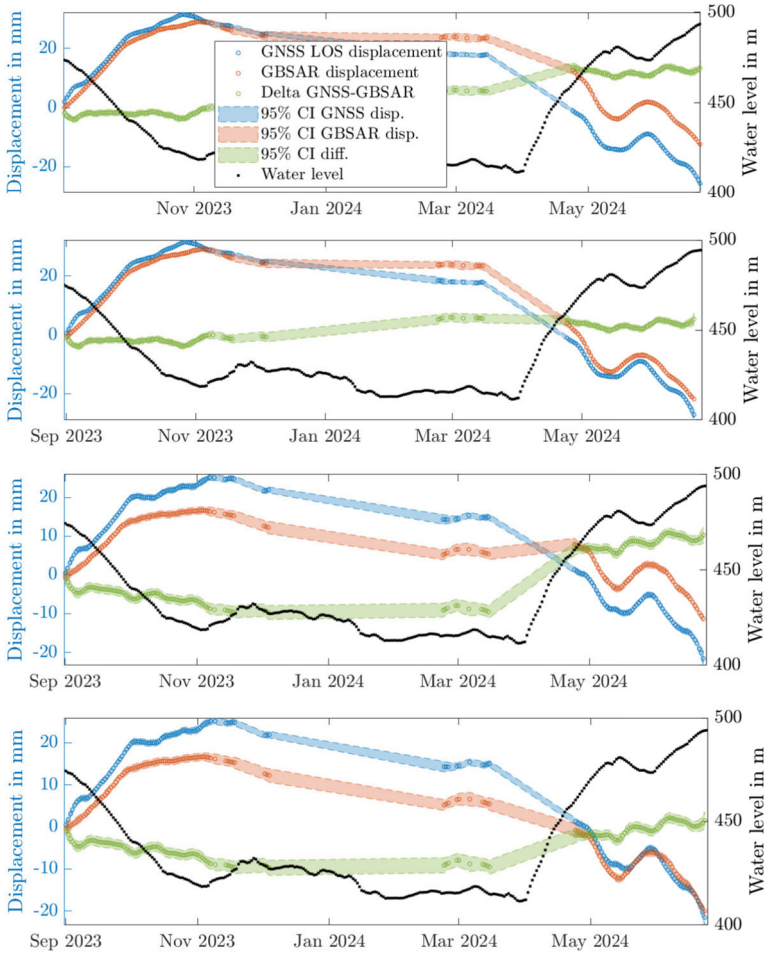

Fig. 3 Synchronized time series before and after the unwrapping correction. In all graphics, the blue points represent the GNSS displacements, red points the GB-SAR displacements and the green points represent the difference. First and second graphs show comparison at the left GNSS before (a) and after (b) correction. Third and last graph show comparison at the right GNSS before (c) and after (d) coretion

are spatially filtered with a median filter with 10 m width, to remove short wavelength patterns in the data that are not represented in the model.

The comparison and difference are shown in the three Figs. 4, 5 and 6. To help the quantification of the difference map, the histograms of the offsets for the three cases are available in Fig. 7, Their key statistics are summarized in Table 1.

From these results, it is clear that the correction of unwrapping errors has been a necessary step, that enabled to reduce the averaged mean offset of half the wavelength. However,

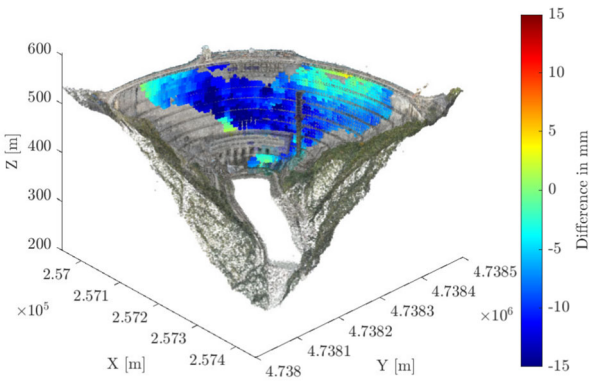

Fig. 4 Difference between the model and the uncorrected GB-SAR data

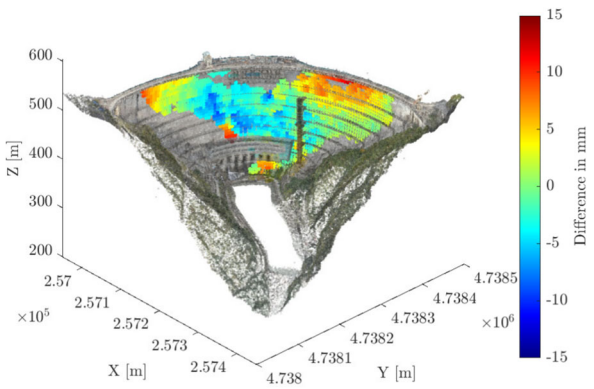

Fig. 5 Difference between the model and the corrected GB-SAR data

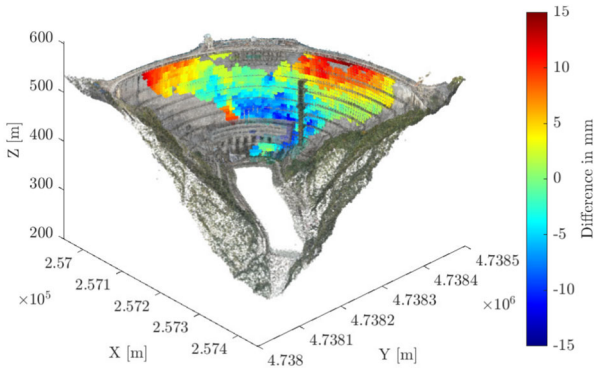

Fig. 6 Difference between the model and the corrected + interpolated GB-SAR data

the interpolation of the residual signal increased the deviation between the model and the resulting estimated displacement map.

Discussion

The bad performances of the interpolation of the residual signal can be explained by the small number of GNSS reference points and their distribution. Indeed, with only two antennas on the dam's crest, and GB-SAR data offsets to be estimated on the whole dam, it is not surprising that it made only diverge the results. What has been achieved is only an interpolation between the two antennas on the dam's crest, but is an extrapolation everywhere else. Therefore, the final displacement map conserved is the one of Fig. 5.

The comparison with a numerical model enables to assess the plausibility of the correction applied. However, it is limited for a precision and accuracy assessment, as the model is only calibrated on eight plumblines across the whole dam. The model can only predict the general displacement pattern. Moreover, the calibration can present offsets up to 30% from the plumblines data. 75% of the relative differences

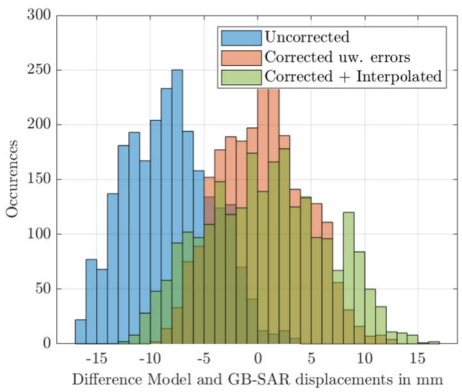

Fig. 7 Histogram of differences between the displacement maps and the model

Table 1 Statistics on the deviations between the model and the different displacement maps

Correction	Mean offset	Std. offset
Uncorrected	−8.3 mm	4.0 mm
Corrected uw. errors	0.4 mm	4.0 mm
Corrected + interp.	0.7 mm	5.7 mm

between the dam and the final displacement map are under 30%. Considering that the calibration period is not the same as the GB-SAR and GNSS observations, these results are satisfying.

Conclusion

The method presented in this paper proposed an efficient way to combine GB-SAR and GNSS data in order to detect unwrapping errors in GB-SAR time series, especially when data interruption occur. The residual displacement between the GNSS and GB-SAR time series is difficult to interpret, but there is apparently no benefits to interpolate onto the whole dam, as it increases the standard deviation to the reference numerical model. Further research to combine different monitoring methods should be undertaken, in order to ensure a consistent monitoring of large infrastructures.

Acknowledgements The authors would like to acknowledge the Bundes Ministerium für Bildung und Forschung for financing the DAMAST and DAMAST Transfer projects.

Author Contributions M.R. and A.S. conceptualize the idea, acquired and processed the GB-SAR data and wrote the main manuscript. M.R. implemented the solution S.H. proposed the idea of the combination of GB-SAR and GNSS data J.W. and M.W. acquired, processed and provided the GNSS data J.W. wrote the GNSS processing description part F.A. and M.V. computed the and provided numerical model.

Funding Open Access funding enabled and organized by Projekt DEAL. This work was partially funded by the BMBF (Bundesministerium für Bildung und Forschung) for the DAMAST (Dams and induced Seismicity Technologies for Risk Reduction) project within the framework of "CLIENT II - International Partnership for Sustainable Innovations," a funding program of the BMBF as part of "Research for Sustainable Development" (FONA). BMBF-Projekt 03G0882A - DAMAST and DAMAST Transfer.

Data Availability No datasets were generated or analysed during the current study.

Declarations

Competing Interests The authors declare no competing interests.

References

Alba M, Bernardini G, Giussani A, Ricci P, Roncoroni F, Scaioni M, Valgoi P, Zhang K et al (2008) Measurement of dam deformations by terrestrial interferometric techniques. Int Arch Photogramm Remote Sens Spat Inf Sci 37(B1):133–139

Bamler R, Hartl P (1998) Synthetic aperture radar interferometry. Inverse Prob 14(4):1

Berardino P, Fornaro G, Lanari R, Sansosti E (2002) A new algorithm for surface deformation monitoring based on small baseline differential sar interferograms. IEEE Trans Geosci Remote Sens 40(11):2375–2383

Bertone A, Seppi R, Callegari M, Cuozzo G, Dematteis N, Krainer K, Marin C, Notarnicola C, Zucca F (2023) Unprecedented observation of hourly rock glacier velocity with ground-based sar. Geophys Res Lett 50(9):2023–102796

Chen CW, Zebker HA (2001) Two-dimensional phase unwrapping with use of statistical models for cost functions in nonlinear optimization. JOSA A 18(2):338–351

Ferretti A, Prati C, Rocca F (2001) Permanent scatterers in sar interferometry. IEEE Trans Geosci Remote Sens 39(1):8–20

Gudmundsson S, Sigmundsson F, Carstensen JM (2002) Three-dimensional surface motion maps estimated from combined interferometric synthetic aperture radar and gps data. J Geophys Res Solid Earth 107(B10):13

Hassan A, Xu J, Zhang L, Liu G, Schmitt A, Xing C, Xu Y, Ouyang C, Schwieger V (2018) Towards integration of gnss and gb-sar measurements: exemplary monitoring of a rock fall at the Yangtze River in China. In: Proceedings of the embracing our smart world where the continents connect: enhancing the geospatial maturity of societies, proceedings of the FIG congress

ICOLD (2020) International Commission on large dams. https://www.icold-cigb.org/GB/world_register/general_synthesis.asp. Accessed 26 Sept 2023

Jacquemart M, Meier L (2014) Deformationsmessungen an talsperren und in deren alpiner umgebung mittels radarinterferometrie. Wasser Energie Luft 106:105–111

Noferini L, Pieraccini M, Mecatti D, Luzi G, Atzeni C, Tamburini A, Broccolato M (2005) Permanent scatterers analysis for atmospheric correction in ground-based sar interferometry. IEEE Trans Geosci Remote Sens 43(7):1459–1471

Qiu Z, Jiao M, Jiang T, Zhou L (2020) Dam structure deformation monitoring by gb-insar approach. IEEE Access 8:123287–123296

Rebmeister M (2024) Geodetic monitoring of complex shaped infrastructures using ground-based insar. PhD thesis, KIT. https://doi.org/10.5445/IR/1000167234

Rebmeister M, Auer S, Schenk A, Hinz S (2022) Geocoding of ground-based sar data for infrastructure objects using the maximum a posteriori estimation and ray-tracing. ISPRS J Photogramm Remote Sens 189:110–127

Rebmeister M, Schenk A, Hinz S, Andrian F, Vonie M (2023) High dam monitoring with ground-based sar: opportunities and challenges. In: ICOLD 2023: 91st ICOLD annual meeting

Scaioni M, Marsella M, Crosetto M, Tornatore V, Wang J (2018) Geodetic and remote-sensing sensors for dam deformation monitoring. Sensors 18(11). https://doi.org/10.3390/s18113682

Tarchi D, Rudolf H, Luzi G, Chiarantini L, Coppo P, Sieber AJ (1999) Sar interferometry for structural changes detection: a demonstration test on a dam. In: IEEE 1999 International Geoscience and Remote Sensing Symposium. IGARSS'99 (Cat. No. 99CH36293). IEEE, vol 3, pp 1522–1524

Wang P, Xing C, Pan X (2020) Reservoir dam surface deformation monitoring by differential gb-insar based on image subsets. Sensors 20(2). https://doi.org/10.3390/s20020396

Wanninger L, Wallstab-Freitag S (2007) Combined processing of gps, glonass, and sbas code phase and carrier phase measurements. In: Proceedings of the 20th international technical meeting of the satellite division of the institute of navigation (ION GNSS 2007), pp 866–875

Wieser A, Condamin S, Barras V, Schmid L, Butt J (2020) Staumauerüberwachung-vergleich dreier technologien für epochenweise deformationsmessungen. Ingenieurvermessung 20. Beiträge zum 19. Internationalen Ingenieurvermessungskurs München 2020:437–449